Michigan Technological University

Michigan Technological University
Digital Commons @ Michigan Tech

Department of Physics Publications | Department of Physics

7-29-2010

Real-time fracture detection of individual boron nitride nanotubes in severe cyclic deformation processes

Hessam Mir Shah Ghassemi
Michigan Technological University

C. H. Lee
Michigan Technological University

Yoke Khin Yap
Michigan Technological University

Reza Shahbazian-Yassar
Michigan Technological University

Follow this and additional works at: https://digitalcommons.mtu.edu/physics-fp

 Part of the Physics Commons

Recommended Citation

Ghassemi, H. M., Lee, C. H., Yap, Y. K., & Shahbazian-Yassar, R. (2010). Real-time fracture detection of individual boron nitride nanotubes in severe cyclic deformation processes. *Journal of Applied Physics, 108*(2), 024314. http://dx.doi.org/10.1063/1.3456083
Retrieved from: https://digitalcommons.mtu.edu/physics-fp/296

Follow this and additional works at: https://digitalcommons.mtu.edu/physics-fp

 Part of the Physics Commons

Journal of Applied Physics

Real-time fracture detection of individual boron nitride nanotubes in severe cyclic deformation processes

Cite as: J. Appl. Phys. **108**, 024314 (2010); https://doi.org/10.1063/1.3456083
Submitted: 15 March 2010 . Accepted: 21 May 2010 . Published Online: 29 July 2010

H. M. Ghassemi, C. H. Lee, Y. K. Yap, and R. S. Yassar

View Online Export Citation

ARTICLES YOU MAY BE INTERESTED IN

Boron nitride nanotubes: Pronounced resistance to oxidation
Applied Physics Letters **84**, 2430 (2004); https://doi.org/10.1063/1.1667278

Elastic modulus and resonance behavior of boron nitride nanotubes
Applied Physics Letters **84**, 2527 (2004); https://doi.org/10.1063/1.1691189

Mechanical strength of boron nitride nanotube-polymer interfaces
Applied Physics Letters **107**, 253105 (2015); https://doi.org/10.1063/1.4936755

Lock-in Amplifiers up to 600 MHz
starting at $6,210


Zurich Instruments
Watch the Video

© 2010 American Institute of Physics.

AIP Publishing

Real-time fracture detection of individual boron nitride nanotubes in severe cyclic deformation processes

H. M. Ghassemi,[1] C. H. Lee,[2] Y. K. Yap,[2,a)] and R. S. Yassar[1,b)]
[1]*Department of Mechanical Engineering-Engineering Mechanics, Michigan Technological University, 1400 Townsend Dr., Houghton, Michigan 49931, USA*
[2]*Department of Physics, Michigan Technological University, 1400 Townsend Dr., Houghton, Michigan 49931, USA*

(Received 15 March 2010; accepted 21 May 2010; published online 29 July 2010)

Real-time deformation of individual multiwalled boron nitride nanotubes (BNNTs) was investigated using an atomic force microscopy (AFM) stage installed inside the chamber of a transmission electron microscopy (TEM) system. These *in situ* AFM-TEM experiments were conducted in following two deformation regimes: a small-angle (~65°) and a large-angle (~120°) cyclic bending process. BNNTs survived from the low-angle test and their modulus was determined as ~0.5 TPa. Fracture failure of individual BNNTs was discovered in the large-angle cyclic bending. The brittle failure mechanism was initiated from the outermost walls and propagated toward the tubular axis with discrete drops of applied forces. © *2010 American Institute of Physics*. [doi:10.1063/1.3456083]

I. INTRODUCTION

Boron nitride nanotubes (BNNTs) possess lattice structures similar to carbon nanotubes (CNTs) but have a large theoretical band gap of ~5.5 eV.[1] These one-dimensional nanostructures are predicted to have exceptional mechanical properties and applicable for high-strength composites. Very few experiments have been performed to date with respect to the experimental examination of mechanical properties of BNNTs. In order to enable the future application of BNNTs in future nanoscale or microscale devices, it is, therefore, important to understand the failure and deformation mechanisms of these nanotubes.

The authors of this manuscript recently conducted a thorough literature review of the theoretical and experimental understanding of BNNT's mechanics.[2] Theoretical studies predict that the Young's modulus of BNNTs can be up to 1.2 TPa.[3,4] Experimentally, the Young's modulus was measured to be ~0.5 TPa using a direct force method[5] and ~0.8 TPa using the electric-field-induced resonance method.[6] Theoretically, a bending angle of ~70° can lead to failure or breaking of B–N bonds in pristine single-wall BNNTs.[7] Recently, Golberg *et al.*[5] reported that at bending angles of ~115°, a residual plastic buckle could remain in the structure of the nanotube. This resulted in the formation of ~30° angled-kinks on BNNTs after unloading. We also recently studied the high temperature structural degradation of BNNTs.[8] In the current research, we investigated the cyclic behavior of BNNTs, an area not previously studied. Our objective was to understand the performance limits of BNNTs under severe bending condition.

II. EXPERIMENTAL PROCEDURE

We have studied the cyclic deformation of individual BNNTs under two different deformation regimes using small-angle (~65°) and large-angle (~120°) cyclic bending. Our experiments were conducted by atomic force microscopy (AFM) under *in situ* monitoring using JEOL JEM-4000FX transmission electron microscopy (TEM) operated at 200 keV. The reliability of such *in situ* AFM/TEM measurements has been well-documented.[5,9,10] Our BNNTs were directly deposited on Si substrates by thermal chemical vapor deposition at 1100–1200 °C in a conventional tube furnace.[11] Powders including MgO, Fe_2O_3, and pure B were used as precursors, and NH_3 gas was used as the source of nitrogen. These BNNTs have a band gap ~5.9 eV, which is higher than those used in previous reports (~5.4 eV), promising the high purity of sample.[5,10] Figure 1 represents a high resolution TEM image of the synthesized BNNTs and the line intensity shown in (b) along the dashed line in (a) indicates that the distance between walls is around 0.35 nm. Individual BNNTs were then attached on a Pd–Au wire (shown in Fig. 2) with silver paste by light mechanical scratching on the as-grown samples. The Pd–Au wire was then fixed on a Au hat, which can be placed on a sapphire ball that enables the coarse motion of the sample toward the AFM tip. The piezotube that is made of stacks of piezocrystal layers enables the fine motion (nanometer resolution) sample toward the AFM tip (Fig. 2). Using the Nanofactory™ software (NFC3), the sample position was adjustable with a precision of 1 nm in *X*, *Y*, and *Z* directions.

III. RESULTS AND DISCUSSION

Figure 3 shows the position of one individual BNNT (~50 nm in diameter) in contact with the AFM tip before, during, and after the bending process. The nanotube was bent at the vicinity of the center, suggesting that there was no imperfection or filled part on the nanotube. Filled nanotubes were shown to deform at the vicinity of the filled part or imperfection sites.[10] The maximum in-plane bending angle in our case was measured as ~65° ± 3° (Fig. 3 at 10 s), which is in good comparison with the 70° angle reported by

a)Corresponding author. Electronic mail: ykyap@mtu.edu
b)Corresponding author. Electronic mail: reza@mtu.edu.

 © 2010 American Institute of Physics

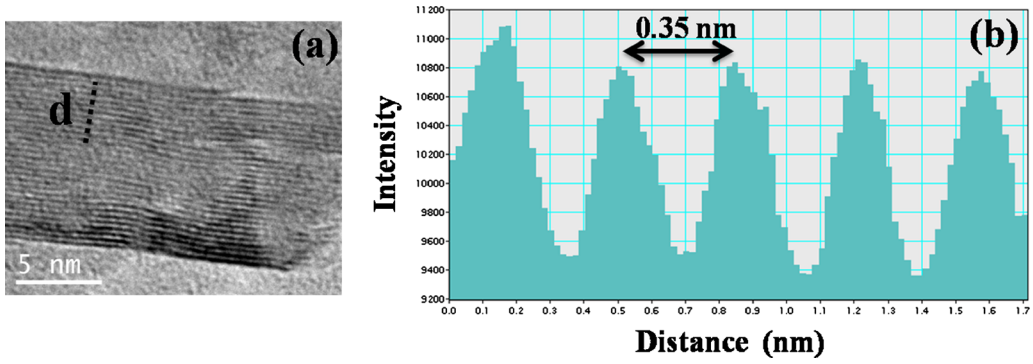

FIG. 1. (Color online) (a) High resolution TEM image of a multiwalled BNNT. (b) The line intensity along the dashed line in (a) indicates that the distance between walls is around 0.35 nm.

Golberg *et al.*[5] for multiwalled BNNTs. For single-walled BNNTs, theoretical simulations by Enyashin and Ivanovskii[7] predicted this angle to be 30°–40°. We found that our nanotube can completely recover its initial tubular structure after unloading from the bending (Fig. 3, released). There was no noticeable defects formation or failure in the structure of this sample even after applying 50 cycles of bending to the same bending angle and unloading.

Figure 4 displays the force-displacement (*F-D*) plots obtained after 1 and 10 bending cycles which corresponds to the 65° of bending deformation. As shown, there was no sudden drop in the applied forces, indicating that the bending cycles introduce no structural failure in the nanotube. There are some deviations between these curves owing to the nanoscopic changes in contact condition between the AFM tip and the nanotube during the loading and unloading cycling processes.

Considering the ionic nature of bonding in BNNTs, one expects to observe a brittle-type behavior. Such high flexibility motivated the authors to conduct a close examination of the bent nanotube in high resolution TEM. Figure 5 corresponds to serious of images that reveal the mechanism by which the BNNTs accommodate high bending angles close to 65°. The dashed lines shown in Fig. 5(c) represent a tilt in atomic planes along a particular set of atoms. The compression, C and tension, T, sides of the nanotube are schematically shown in the inset of Fig. 5(a). In several locations along the compressive side of the nanotube these tilted planes were observed in Fig. 5(b). This mechanism was highly reversible and, after unloading, no sign of tilted plane could be detected.

Using the maximum applied forces in the *F-D* curves, the Young's modulus of nanotubes can be estimated based on the Euler's formula for nanotubes assuming that both ends are fixed,[12] where the maximum applied force is $F_{\text{Euler}} = \pi^2 EI/L^2$. Here, L is the length of the BNNT between the two contacts (=1.5 μm), E is the elastic modulus, and the moment of inertial,

$$I = \frac{\pi(d_2^4 - d_1^4)}{64},$$

where d_1 and d_2 are the internal and external BNNT diameters, respectively. Table I shows the calculations for five different nanotubes. The average Young's modulus detected here was ~0.5 TPa ± 0.1 TPa. The data were reproducible after multiple tests with different individual BNNTs.

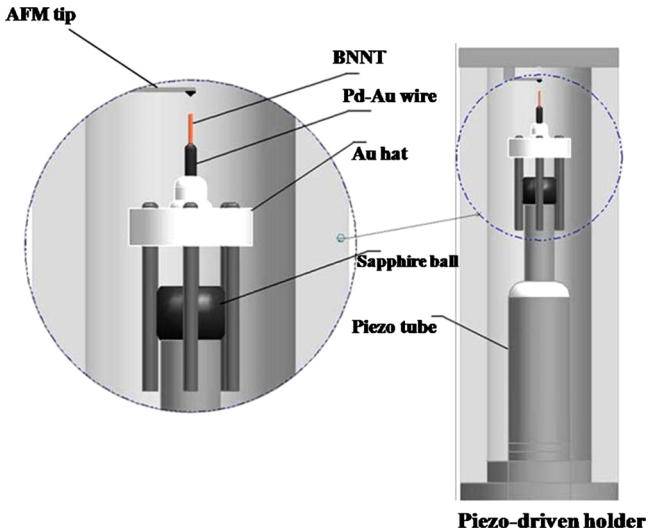

FIG. 2. (Color online) Schematic of the *in situ* AFM setup inside the TEM. BNNTs were placed on the Pd–Au wire and brought into contact with the AFM cantilever through movement of the piezotube and sapphire ball.

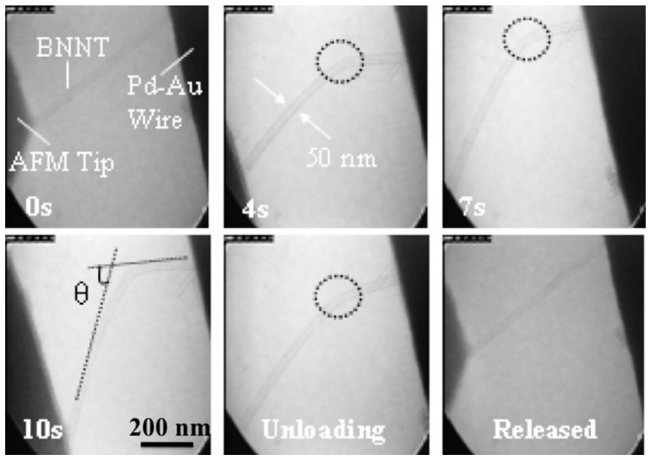

FIG. 3. *In situ* TEM observation shows small-angle (~65°) bending of an individual BNNT at 300 nm displacement within 10 s. Bending point (circled) appears near the middle of the nanotube and is fully recovered upon releasing the applied force. The images captured from the recorded video.

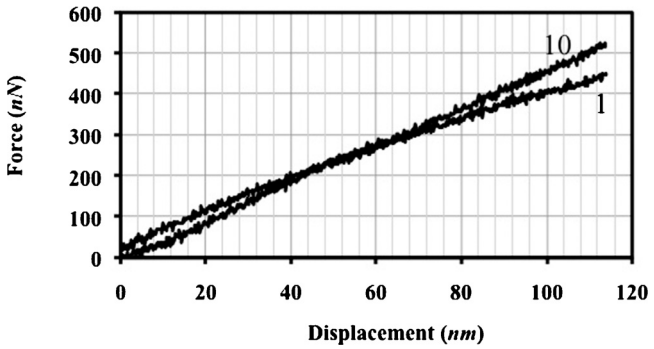

FIG. 4. *F-D* curves during the cyclic bending deformation of an individual BNNT at deformation cycles of 1 and 10.

For the large-angle bending tests, we increased the deformation angle up to 120° to capture the pertinent structural changes. Interestingly, BNNTs failed in a fracture mode. Figure 6 shows the represented real-time process of the failure of an individual BNNT after numerous cycling bending. The *F-D* curve corresponding to this fracture event illustrates the changes in the force applied to the nanotube [Figs. 6(a)–6(e)]. We have recorded three discrete drops in applied forces. The first drop, at the beginning of the experiment, is due to the nanoscopic sliding of the nanotube on the AFM tip. This results in the drop of the applied force. The other two drops (~200 nN each) represent the process of failure initiation and propagation in the nanotube shell-walls [Figs. 6(c)–6(e)]. As the TEM images show, the fracture initiates from the outermost shells [Fig. 6(c)] that are under tensile stress and propagates [Fig. 6(e)] toward the axis of nanotube, almost perpendicular to the applied force axis. As this particular BNNT has a wall thickness ~12 nm, this nanotubes was having ~36 layers of hexagonal boron nitride (*h-BN*) shells. Since the fracture processes initiated only two discrete drops of applied forces within this particular cycle of bending, apparently multiple *h-BN* shells are broken simultaneously in two patches resembling a brittle-type fracture. It is noted that a few layers of shells still remained after this bending cycle as shown in Fig. 6(e). By repeating the bending cycles [Figs. 6(f)–6(h)], the nanotube was eventually broken into two parts [Fig. 6(i)].

We think that the rupturing in the outermost shells may be initiated by structural imperfections such as the Stone–Wales defects.[13] Yu *et al.*[14] reported the breakage of multi-walled CNTs (MWCNTs) in the outermost layer. They assumed that structural defects, such as Stone–Wales, produced during the synthesis process, were responsible for the fracture. Espinosa *et al.*[15] also reported failure of outer shells of MWCNTs as a function of irradiation dose. Ding *et al.*[16] also observed similar failure mechanism. They estimated that defects in the outer shell can cause stress concentrations and thus failure.

TABLE I. The estimated structural parameters for five different BNNTs and the calculated Young's modulus and standard deviation are shown.

	d_1 (nm)	d_2 (nm)	L (nm)	F (nN)	Elastic modulus (TPa)
Nanotube 1	34	51	1400	600	0.45
Nanotube 2	29	44	1600	390	0.68
Nanotube 3	25	50	1500	600	0.48
Nanotube 4	26	48	1800	420	0.58
Nanotube 5	22	38	1300	350	0.66

We then examined the cross-section of the fractured nanotube by using the broken segment 2 to lift the other segment 1. As shown in Fig. 7, we used segment 2 to rotate segment 1 so that the cross-section is perpendicular to the electron beam. Figures 7(a)–7(c) demonstrate this manipulation. In Fig. 7(d), the broken cross-section (marked in a circle) is shown as a ring shape, indicating the presence of the tubular structures. The inner channel at the center of the broken cross-section can be clearly observed. The diameters of the two broken parts were almost similar [Fig. 7(d)] suggesting that the breakage of the nanotube shells is brittle. This is in agreement with the existing belief about BNNT brittleness due to the partially-ionic character of chemical bonding between the B and N atoms.

IV. CONCLUSIONS

In summary, we tested the mechanical properties of individual BNNTs by cyclic bending using an *in situ* AFM/TEM system. The structures of BNNTs remained after the low-angle (~65°) cyclic bending. For the high-angle (~120°) cyclic bending, *in situ* TEM imaging allowed the real-time recording of the shell-walls failure initiation and propagation process. Brittle failure mechanism was observed for bending failure of BNNTs. The drops of the measured

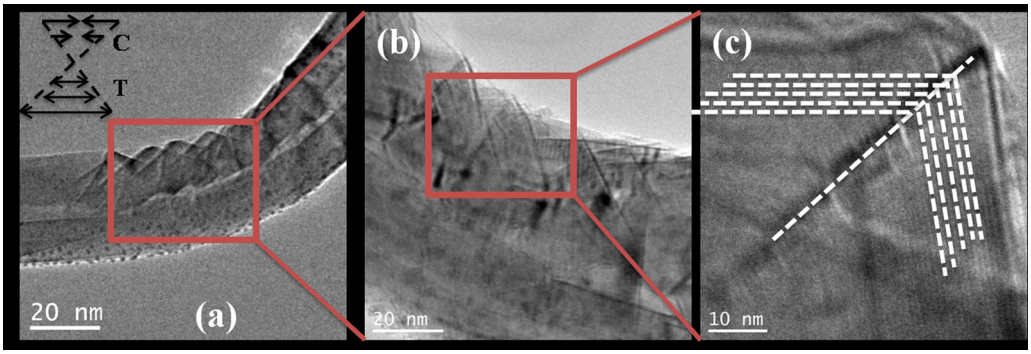

FIG. 5. (Color online) TEM images of a BNNT at the bended area reveal the mechanism by which the nanotubes accommodate high bending angles close to 65°. The compression, C, and tension, T, sides of the nanotube are schematically shown in the inset of (a). The dashed lines shown in (c) represent a tilt in atomic planes along a particular set of atoms.

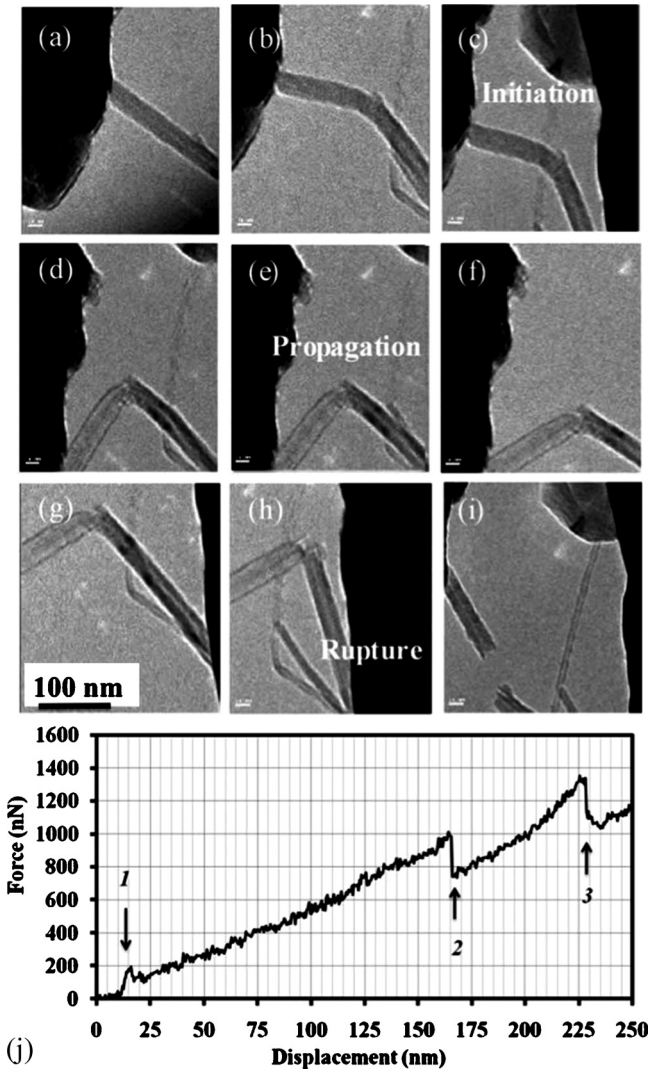

FIG. 6. Process of fracture in an individual BNNT after the large-angle (~120°) bending cycles. [(a)–(e)] Represent one cycle of bending. [(f)–(i)] Showing nanotube breaking into two parts after pulling and stretching. (j) *F-D* plot represents the changes in force upon failure initiation and propagation during one cycle (a)–(e). Scale bars are 20 nm.

force corresponding to the failure of shell-walls determined the contribution of shell-walls on the overall strength of nanotubes.

ACKNOWLEDGMENTS

R. S. Yassar and Y. K. Yap acknowledge support from National Science Foundation (Award No. 0820884, Division of Materials Research). R.S.Y. would like to thank the Michigan Space Grant Consortium Fund for providing the partial of financial support (MSGC under Grant No. 2000433) to conduct the current investigation. Y. K. Yap acknowledges his National Science Foundation *CAREER* award (Award No. 0447555) and the U.S. Department of Energy, the Office of Basic Energy Sciences (Grant No. DE-FG02-06ER46294) for supporting the efforts on the synthesis of boron nitride nanotubes.

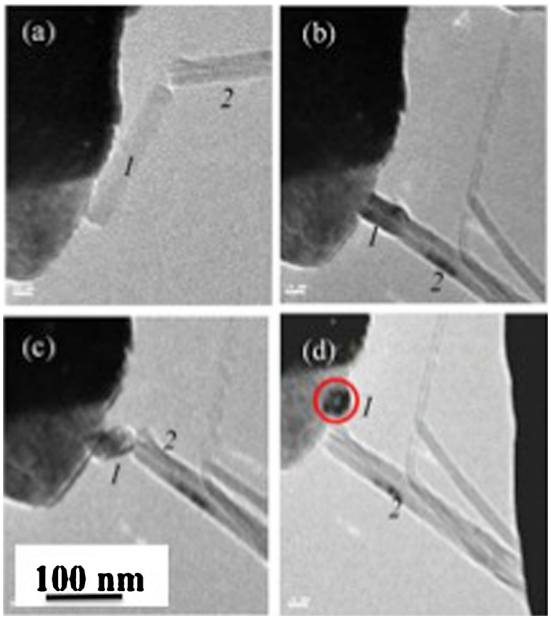

FIG. 7. (Color online) (a)–(c) Manipulation of the broken BNNT on the left (1) using the broken segment on the right (2). (d) Cross-section view of the broken nanotube as marked in a circle. The empty area at the center represents the inner channel of the BNNT. Scale bars are 20 nm.

[1]X. Blase, A. Rubio, S. G. Louie, and M. L. Cohen, Europhys. Lett. **28**, 335 (1994).
[2]H. M. S. Ghassemi and R. S. Yassar, Appl. Mech. Rev. **63**, 020804 (2010).
[3]V. Verma, V. K. Jindal, and K. Dharamvir, Nanotechnology **18**, 435711 (2007).
[4]E. Hernández, C. Goze, P. Bernier, and A. Rubio, Phys. Rev. Lett. **80**, 4502 (1998).
[5]D. Golberg, X. D. Bai, Y. Bando, C. Y. Zhi, C. C. Tang, M. Mitome, and K. Kurashima, Nano Lett. **7**, 2146 (2007).
[6]A. P. Suryavanshi, M. Yu, J. Wen, C. Tang, and Y. Bando, Appl. Phys. Lett. **84**, 2527 (2004).
[7]A. N. Enyashin and A. L. Ivanovskii, Neorg. Mater. **42**, 1336 (2006).
[8]H. M. S. Ghassemi, C. H. Lee, Y. K. Yap, and R. S. Yassar, JOM **62**, 69 (2010).
[9]H. Ghassemi, Y. K. Yap, and R. S. Yassar, Tech. Proc. 2009 Nanotech. Conf. Expo, NSTI Nanotech. **1**, 318 (2009).
[10]D. Golberg, X. D. Bai, M. Mitome, C. C. Tang, C. Y. Zhi, and Y. Bando, Acta Mater. **55**, 1293 (2007).
[11]C. H. Lee, J. Wang, V. K. Kayatsha, J. Y. Huang, and Y. K. Yap, Nanotechnology **19**, 455605 (2008).
[12]S. Akita, H. Nishijima, T. Kishida, and Y. Nakayama, Jpn. J. Appl. Phys., Part 1 **39**, 3724 (2000).
[13]A. J. Stone and D. J. Wales, Chem. Phys. Lett. **128**, 501 (1986).
[14]M. Yu, O. Lourie, M. J. Dyer, K. Moloni, T. F. Kelly, and R. S. Ruoff, Science **287**, 637 (2000).
[15]H. D. Espinosa, Z. Yong, and N. Moldovan, J. Microelectromech. Syst. **16**, 1219 (2007).
[16]W. Ding, L. Calabri, K. M. Kohlhaas, X. Chen, D. A. Dikin, and R. S. Ruoff, Exp. Mech. **47**, 25 (2007).